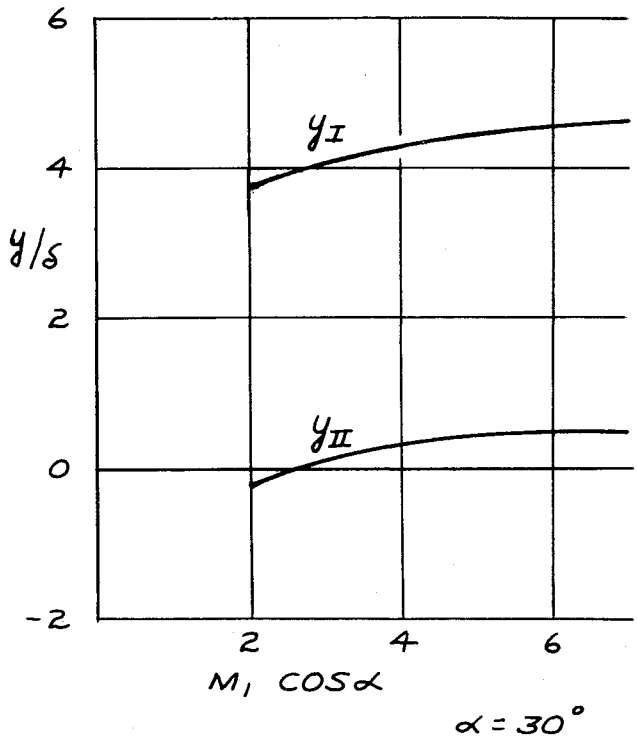

Fig. 3. y/δ vs normal component of M_1.

constant and equal to that immediately behind the shock. The error introduced by this assumption is quite small.

Now $k = 2\rho_1/(\rho_2 + \rho_{2i})$ is a function only of $M_1 \cos\alpha$, and D and E are similarly dependent. Also from Ref. 3

$$\frac{T_2}{T_1} = \frac{[2\gamma M_1^2 \cos^2\alpha - (\gamma - 1)][(\gamma - 1)M_1^2 \cos^2\alpha + 2]}{(\gamma + 1)^2 M_1^2 \cos^2\alpha} \tag{10}$$

It is thus seen that y_I/δ and y_{II}/δ are functions only of M_1 and α. These two nondimensional parameters are plotted in Fig. 3 as a function of M_1 for $\alpha = 30°$.

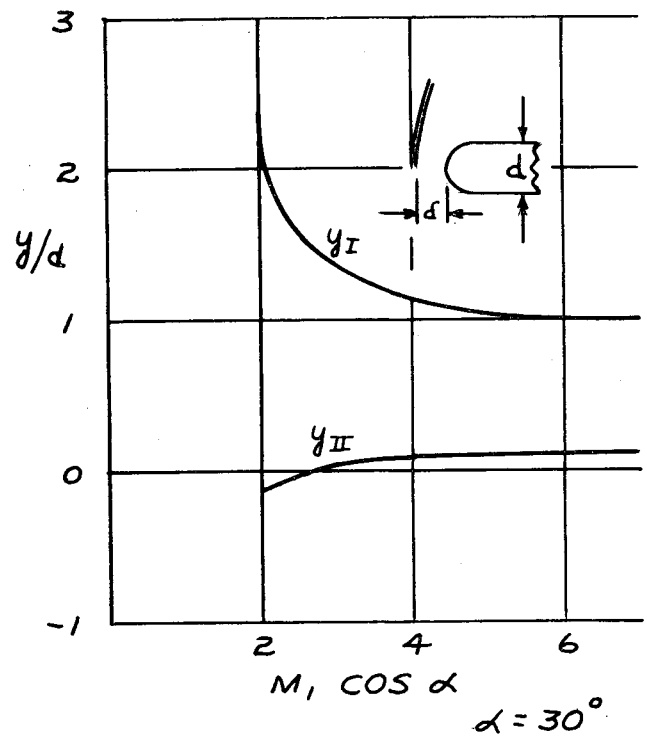

Fig. 4 y/d vs normal component of M_1.

Liepmann and Roshko[4] present a compilation of experimental data for δ/d as a function of Mach number for a cylindrical leading edge. This data was used and values of y_I/d and y_{II}/d were determined, and are shown as a function of M_1 for $\alpha = 30°$ in Fig. 4. From this figure it can be seen that the maximum width of the zone of increased heating is approximately constant for normal Mach numbers greater than 5, and has a magnitude of less than one leading edge diameter. It is noted that at very high altitudes, where the mean free path is large, the value of τ, the impinging shock thickness, becomes substantial and should be considered in estimating the width of the interaction zone.

Conclusions

Combining the experimental data of Ref. 1 with the foregoing analysis, a method to predict the effect of shock interaction on leading edge heating is available. Lacking experimental verification, this method is only a promising approach.

References

[1] Newlander, R. A., "Effect of shock impingement on the distribution of heat-transfer coefficients on a right circular cylinder at Mach numbers of 2.65, 3.51, and 4.44," NASA TN D-642 (January 1961).

[2] Truitt, R. W., *Hypersonic Aerodynamics* (The Ronald Press Co. New York, 1959), pp. 236–242.

[3] Ames Research Staff, "Equations, tables, and charts for compressible flow," NACA Rept. 1135 (1953).

[4] Liepmann, H. W. and Roshko, A., *Elements of Gasdynamics* (John Wiley and Sons, Inc., New York, 1957), p. 105.

Simulation of the Interaction of a Hypersonic Body and a Blast Wave

GENE J. BINGHAM* AND THEODORE E. DAVIDSON†
North American Aviation, Inc., Columbus, Ohio

A TRANSIENT pressure rise will be produced at the surface of a hypersonic body intersected by a blast wave. The transient pressure will be a function of the strength of the body wave and the blast wave plus the attitude of the interacting waves. The general characteristics of body waves and blast waves have been defined individually. However, the interaction effects of the two wave systems have not been completely defined. The investigation described here was initiated to establish the feasibility of a technique to simulate and to measure the interaction of a blast wave and a hypersonic body.

A model mounted in a continuous hypersonic wind tunnel simulated the hypersonic body. A shock tube was selected to simulate the blast wave because 1) the strength of the traveling shock wave is controllable and repeatable, 2) safety problems are minimized, 3) a shock tube can be added to open jet tunnels, 4) the physical parameters associated with shock tubes are well known, and 5) feasibility of this technique had been demonstrated with a supersonic wind tunnel with a solid jet boundary.[1]

It is noted that, although a supersonic tunnel-shock tube arrangement permitted an investigation of shock interaction, the feasibility with a hypersonic wind tunnel had not been established. In particular, the question remained as to

Received October 26, 1964. Effort was conducted under U. S. Air Force Contract AF33(657)-10786, Project No. 1350, Task No. 135001; monitored by Flight Dynamics Laboratory, Wright-Patterson Air Force Base, and supported by the Defense Atomic Support Agency.

* Senior Technical Specialist, Advanced Environmental Development Group. Member AIAA.

† Senior Engineer, Advanced Environmental Development Group.

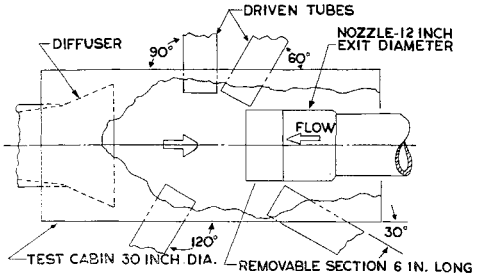

Fig. 1 Tunnel-shock tube schematic.

whether or not a shock propagated through the free-jet boundary of a hypersonic stream would intersect a model immersed in the stream.

The present investigation was conducted in the Ohio State University Aerodynamic Laboratory's 12-in. hypersonic wind tunnel.[2] The basic tunnel components included a stagnation chamber with an electric resistance air heater, a 12-in.-diam Mach-7 nozzle, and a diffuser-evacuation system. The tunnel was modified by replacing the conventional test cabin with a 30-in.-diam pipe with attached shock tubes (Fig. 1).

The shock tubes, which were approximately 6 in. i.d., were installed at angles of 30°, 60°, 90°, and 120° with respect to the tunnel centerline. For the 30° and 60° shock tubes, a 6-in. section of the nozzle was removed to avoid interference with the traveling shock wave. A double diaphragm arrangement was used to separate the driver and driven tubes. Air or helium was used in the driver to develop shock velocities (Vs) between 3600 and 7300 fps. An air-hydrogen mixture was burned in the driver to obtain a shock velocity of approximately 13,500 fps. The driven tubes were instrumented with thin film platinum gages for measurement of the moving shock velocity.

A 60° angle blunted cone model with a 3-in.-diam base and $\frac{1}{2}$-in. nose radius was attached to a mechanism that would rotate the model into and out of the stream. This mechanism also permitted the model to be moved in a streamwise direction to provide proper alignment with the shock tube.

Piezoelectric pressure transducers were mounted 1.8 and 2.5 in. from the imaginary vertex of the cone and flush with the surface. All instrumentation readouts were displayed on oscilloscopes and photographically recorded.

A schlieren arrangement with a multiple spark light source was used to photograph the traveling shock and the shock wave interaction. The light source, which is similar to one described in Ref. 3, uses five barium titanate capacitors with spark gaps mounted in series and focused by a lens assembly. Electrodes attached to the poles of each capacitor generate a spark when the capacitor is discharged across the electrodes. Capacitor discharge was initiated by an electronic timing circuit.

A test run was initiated by moving the model into the stream and starting the following sequence of events: 1) the model actuator arm opened a switch releasing the double diaphragm gas, 2) the diaphragms ruptured and the shock wave was generated, 3) the traveling wave was sensed by the shock tube instrumentation, and 4) the oscilloscopes and multiple spark timing circuit were triggered for operation.

Photographs of the moving shock wave without tunnel air flow indicate that the shock wave moves from the shock tube in a manner similar to that shown in Fig. 2. The axis of the moving shock wave coincides with the shock tube centerline. The quasisteady flow field behind the incident shock wave generated a standing wave at the model (not indicated). This flow continued until the arrival of the driver tube gas. The pressure distribution over the model would be approximately constant for the duration of the quasisteady flow.

The shock waves observed with tunnel flow at Mach 7.3 (Fig. 3) are basically similar to those for the tunnel-off case. However, it will be noted that the spacing between shock

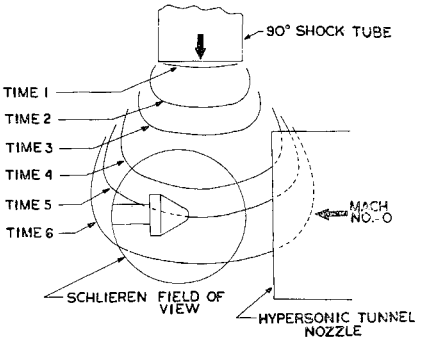

Fig. 2 Development of the incident shock, no tunnel flow.

waves increases in a stream direction. This increase indicates that the wave is swept downstream by the tunnel air flow. The maximum shifting of the wave was observed with the 30° shock tube operating at low shock velocities. In fact, for this case, part of the shock wave was swept parallel to the model.

In some instances, the shock waves shown by a given spark appeared as a number of lines. This apparent multiple wave form is associated with the effects of the jet boundary on the moving shock wave. As indicated in Ref. 4, the velocity of the shock would be expected to increase as it crosses the free-jet boundary into the cooler hypersonic stream. In the present case, the jet boundary is cylindrical so that the initial segment of the moving shock wave which crosses the cylinder is amplified first. The segments of the moving shock, off the axis of this initial segment, pass at a slightly later time and at a slightly different angle relative to the cylindrical jet boundary. Therefore, there is a variation in wave amplification and wave displacement. Realizing that the schlieren system records tangents to shock waves, it is concluded that the single moving wave has a number of tangency points. By observation, the wave distortion appears small compared with the major dimensions of the model. Therefore, it is believed that the moving wave is satisfactory for shock interaction simulation for the range of this investigation.

The pressures measured on the model remained constant

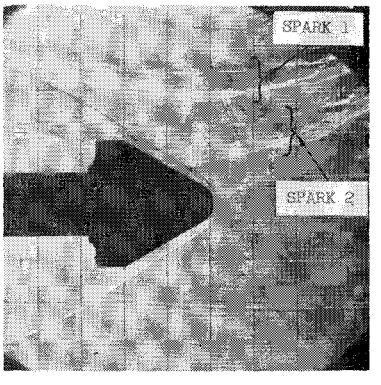

Fig. 3a Shock tube at 90°, Vs ~ 6000 fps.

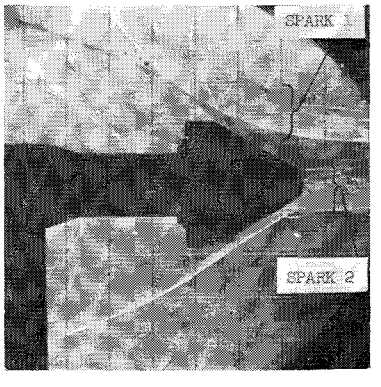

Fig. 3b Shock tube at 60°, Vs ~ 6000 fps.

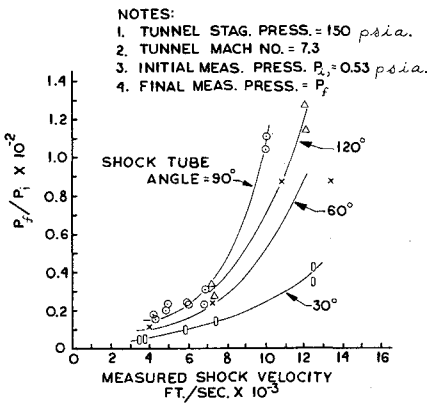

Fig. 4 Variation of model pressure ratio with shock velocity.

until the shock wave intersected the instrumentation. At intersection, a step change in pressure was observed. As would be expected, the pressure ratio increases with increasing shock velocity (Fig. 4). The pressure ratio varies from a maximum with the 90° shock tube to a minimum with the 30° tube. The variation is attributed to the attitude of the transducers relative to the advancing shock front and to variations in distance from the shock tube exit to the model.

It is concluded that the technique described in this paper provides a feasible method for simulating the interaction of a blast wave with a hypersonic body. It is also feasible to measure pressure-time histories on the body.

References

[1] Pierce, D., "Simulation of blast waves in a supersonic wind tunnel," Royal Aircraft Establishment TN AERO 2665 (January 1960).

[2] Thomas, R. E. and Lee, J. D., "The Ohio State University 12-inch hypersonic wind tunnel system," The Ohio State Univ. Rept. TN (ALOSU), pp. 559–562 (July 1959).

[3] Wilson, M. R. and Hienmenz, R. J., "Light source for high-speed photography," Research Trends Cornell Aeronautical Lab. Rept. Vol. VII (1959).

[4] Bitondo, D., Glass, I. I., and Patterson, G. N., "One dimensional theory of absorption and amplification of a plane shock wave by a gaseous layer," Univ. of Toronto Institute of Aerophysics Rept. 5, pp. 17–21 (June 1950).

Uniformly Loaded Plates of Regular Polygonal Shape

A. W. Leissa,* C. C. Lo,† and F. W. Niedenfuhr*
The Ohio State University, Columbus, Ohio

In a previous note Niedenfuhr and Leissa[1] used the point-matching method to determine torsional stresses and rotations of bars having regular polygonal cross sections. The present note summarizes results obtained in applying the method to the bending of uniformly loaded plates of regular polygonal shape with sides either clamped or simply supported.

The differential equation of equilibrium to be solved is

$$D\nabla^4 w = q_0 \tag{1}$$

Received November 2, 1965. The results contained in this note are a partial product of research supported by the U. S. Air Force under Contract No. AF33(657)8772, monitored by G. E. Maddux, ASRMDS-22, Wright Patterson Air Force Base.

* Professor, Department of Engineering Mechanics. Associate Fellow Member AIAA.

† Research Associate, Department of Engineering Mechanics.

Table 1 Deflections and moments; clamped edges

No. of sides, m	wD/q_0a^4 at $r = 0$	M/q_0a^2 at $r = 0$	M_x/q_0a^2 at $r = a, \theta = 0$
3	0.02414	0.09812	−0.2372
4	0.02024	0.09162	−0.2053
5	0.01861	0.08832	−0.1886
6	0.01774	0.08640	−0.1780
7	0.01722	0.08519	−0.1705
8	0.01687	0.08436	−0.1650
9	0.01663	0.08377	−0.1607
10	0.01645	0.08334	−0.1573
∞	0.01562	0.08125	−0.1250

where D is the flexural rigidity, ∇^4 is the biharmonic differential operator, w is the transverse deflection, and q_0 is the uniform transverse loading. An exact solution to Eq. (1) will be taken in polar coordinates as

$$w = \sum_{n=0}^{N} (A_n r^n + B_n r^{n+2}) \cos n\theta + \frac{q_0 r^4}{64D} \tag{2}$$

where the coefficients A_n and B_n are to be determined from the boundary conditions and the upper limit of summation N is determined by the accuracy of solution desired from the point matching process.

Typical plate geometry is exemplified by Fig. 1, wherein the special case of a hexagonal boundary is shown. The plate centroid is used as coordinate origin and θ is measured from a symmetry axis bisecting a side. The plate dimension is measured by denoting the radius of the inscribed circle as "a."

Taking advantage of the manifold symmetry present, the summation index n is taken successively as $0, m, 2m, 3m, \ldots$, where m is the number of sides for a particular regular polygon. The boundary conditions for all problems were applied at nine equally spaced points (including midpoints and vertices) in one sector subtended by the angle π/m as shown in Fig. 1. By symmetry considerations then, these boundary conditions are enforced in all $2m$ sectors of the polygon.

Clamped edge conditions were obtained by choosing $N = 8m$ and requiring the deflection and its normal derivative to be zero at the nine points. Solution of the resulting 18 simultaneous equations determines the coefficients A_n and B_n. Bending moments are evaluated by proper combination of second derivatives of deflection. The problem formulation, solution, and evaluation were accomplished automatically by means of a general-purpose computer program and significant results for $m = 3, 4, \ldots 10$ are presented in Table 1.

The accuracy of these solutions may be judged by two criteria: 1) the maximum deviation from exact boundary conditions between points matched, and 2) the rate of convergence of solutions as the number of boundary points used is changed. In Table 1, the maximum deviation from zero deflection along the boundary occurs in the case of the triangle

Table 2 Deflections, slopes, and moments; simply supported edges

No. of sides, m	wD/q_0a^4 at $r = 0$	M/q_0a^2 at $r = 0$	$D(\partial w/\partial x)/q_0a^3$ at $r = a, \theta = 0$
3	0.0833	0.217	−0.1406
4	0.0650	0.192	−0.1078
5	0.0581	0.181	−0.0942
6	0.0548	0.176	−0.0871
7	0.0532	0.174	−0.0833
8	0.0525	0.173	−0.0813
9	0.0523	0.173	−0.0803
10	0.0523	0.174	−0.0798
15	0.0537	0.179	−0.0809
∞	0.0637	0.206	−0.0962